Macroscale water fluxes
3. Effects of land processes on variability of monthly river discharge

P. C. D. Milly

U. S. Geological Survey and Geophysical Fluid Dynamics Laboratory, NOAA, Princeton, New Jersey, USA

R. T. Wetherald

Geophysical Fluid Dynamics Laboratory, NOAA, Princeton, New Jersey, USA

Received 9 July 2001; revised 15 April 2002; accepted 15 April 2002; published 15 November 2002.

[1] A salient characteristic of river discharge is its temporal variability. The time series of flow at a point on a river can be viewed as the superposition of a smooth seasonal cycle and an irregular, random variation. Viewing the random component in the spectral domain facilitates both its characterization and an interpretation of its major physical controls from a global perspective. The power spectral density functions of monthly flow anomalies of many large rivers worldwide are typified by a "red noise" process: the density is higher at low frequencies (e.g., $<1\ y^{-1}$) than at high frequencies, indicating disproportionate (relative to uncorrelated "white noise") contribution of low frequencies to variability of monthly flow. For many high-latitude and arid-region rivers, however, the power is relatively evenly distributed across the frequency spectrum. The power spectrum of monthly flow can be interpreted as the product of the power spectrum of monthly basin total precipitation (which is typically white or slightly red) and several filters that have physical significance. The filters are associated with (1) the conversion of total precipitation (sum of rainfall and snowfall) to effective rainfall (liquid flux to the ground surface from above), (2) the conversion of effective rainfall to soil water excess (runoff), and (3) the conversion of soil water excess to river discharge. Inferences about the roles of each filter can be made through an analysis of observations, complemented by information from a global model of the ocean-atmosphere-land system. The first filter causes a snowmelt-related amplification of high-frequency variability in those basins that receive substantial snowfall. The second filter causes a relatively constant reduction in variability across all frequencies and can be predicted well by means of a semiempirical water balance relation. The third filter, associated with groundwater and surface water storage in the river basin, causes a strong reduction in high-frequency variability of many basins. The strength of this reduction can be quantified by an average residence time of water in storage, which is typically on the order of 20–50 days. The residence time is demonstrably influenced by freezing conditions in the basin, fractional cover of the basin by lakes, and runoff ratio (ratio of mean runoff to mean precipitation). Large lake areas enhance storage and can greatly increase total residence times (100 to several hundred days). Freezing conditions appear to cause bypassing of subsurface storage, thus reducing residence times (0–30 days). Small runoff ratios tend to be associated with arid regions, where the water table is deep, and consequently, most of the runoff is produced by processes that bypass the saturated zone, leading to relatively small residence times for such basins (0–40 days). *INDEX TERMS:* 1818 Hydrology: Evapotranspiration; 1854 Hydrology: Precipitation (3354); 1860 Hydrology: Runoff and streamflow; *KEYWORDS:* temporal variability, spectral analysis, snowmelt, storage, residence time

Citation: Milly, P. C. D., and R. T. Wetherald, Macroscale water fluxes, 3, Effects of land processes on variability of monthly river discharge, *Water Resour. Res.*, *38*(11), 1235, doi:10.1029/2001WR000761, 2002.

1. Introduction

1.1. Motivation

[2] The expected value of discharge of a river varies through the year, following the seasonal cycles of such climatic variables as precipitation, solar radiation, and air temperature. Superimposed upon this variation are random (chaotic) fluctuations at all timescales, reflecting everything from decadal changes in the state of the climate system to the rapid passage of a convective storm cell. The relative strengths of these random variations, in turn, vary from one basin to another around the globe. Much of hydrology is

concerned with description and prediction of this variability, which so frequently manifests itself in floods and droughts. At the same time, a quantitative grasp of natural variability is a prerequisite for rigorous assessment of the significance of recent and future changes in river flow.

[3] Many random process models have been applied in the analysis of flow variability [*Bras and Rodríguez-Iturbe*, 1985]. Use of such models, for example, to generate artificial time series for engineering design, has long been commonplace. Perhaps because of the wide variety and sophistication of such models and the site-specific and goal-specific nature of such applications, however, no comprehensive synthesis of the diverse results has been attempted, and our global- scale understanding of river flow variability remains limited.

[4] Furthermore, random process models and their fitted parameters are rarely interpreted in terms of the physical processes that produce river flow. Nevertheless, the forcing of flow variations by weather and climatic variations is self-evident. How are precipitation fluctuations modulated by the various components of the land-surface hydrologic system? What are the climatic and physiographic controls on the relevant processes? How can these factors be modeled quantitatively? These are some of the questions that motivate the present study.

[5] This work is also motivated by the need to characterize river discharge in global models of the land-ocean-atmosphere system. Applications of such models to climate simulation and associated hydrologic analysis generally focus on basins that can be resolved by the models (e.g., greater than 10,000 km^2 in area) at timescales characterizing variability of discharge from basins of such sizes.

1.2. Objectives of These Papers

[6] This is the third in a series of three papers analyzing controls on water balances of large land areas. Part 1 [*Milly and Dunne*, 2002a] describes the development of the data set upon which the subsequent papers are based, with special attention to assessment of errors in estimates of precipitation. In part 2 [*Milly and Dunne*, 2002b], these data are employed to analyze the control of interannual water balance variations by fluctuations in supplies of water (precipitation) and energy (surface net radiation). In the present paper (part 3), the data of part 1 and the results of part 2 are used to develop and quantify a conceptual picture of land-process controls of monthly streamflow variability.

[7] More specifically, the objectives of this paper are to characterize the random component of temporal variability of monthly discharge from river basins and to identify the dominant physical controls of that variability. The emphasis here on the monthly (as opposed to daily or shorter) timescale is driven by three factors: (1) the relative ease of access to monthly flow and precipitation data on a global scale, (2) the relatively high attenuation of flow anomalies for medium to large basins at frequencies higher than those associated with the monthly timescale, and (3) the desire to avoid a detailed analysis of the surface drainage network that is needed to interpret such higher-frequency (e.g., daily) flows.

2. Data

2.1. Observational Data

[8] We use the river-basin data set of part 1. The data set includes continuous, long-term (median record length 54 years) monthly time series of precipitation and discharge for 175 large (median area 51,000 km^2) basins worldwide. The basin mean precipitation was estimated by interpolation of point gauge values. Part 1 also quantified the uncertainty in their estimates of basin mean precipitation. In the notation of part 1, statistical behavior of relative errors in the long-term annual mean were summarized by a parameter ψ_a,

$$\psi_a = \left[E\{\varepsilon_a^2\}\right]^{1/2}/\langle \hat{p}_a \rangle \tag{1}$$

in which $E\{\}$ represents the expected value of a random process, p_a denotes long-term-mean annual total precipitation amount, circumflex denotes a gauge-based estimate, angle brackets denote areal average over a river basin, and ε_a is the error in the estimate of long-term basin mean annual precipitation, $\langle \hat{p}_a \rangle$. Components of ε_a considered include expected spatial-sampling errors in the absence of orographic effects, spatial-sampling errors associated with orographic effects, and errors in adjustments for gauge bias. In part 1, standard correlation-based methods were also applied to develop estimates of the standard errors of anomalies from the mean during any particular month or year. As a summary measure of the anomaly errors, part 1 introduced the parameter $\overline{\psi_n}$,

$$\overline{\psi_n} = \overline{\sigma_n^2}/\mathrm{Var}(\langle P_n \rangle), \tag{2}$$

in which σ_n^2 is the variance of the error in the estimate of the basin mean anomaly for year n, an overbar denotes an average over the period of record, and $\mathrm{Var}(\langle P_n \rangle)$ is the variance of the basin mean annual precipitation. Because both the precipitation and the error of estimation of its anomaly are nearly uncorrelated in time at the monthly level, the index $\overline{\psi_n}$ is also approximately equal to the time-average ratio of variance of the error of monthly precipitation anomalies to the variance of monthly precipitation.

[9] In this analysis, we focus on temporal variability much more than on mean values. Accordingly, we are more concerned with minimizing $\overline{\psi_n}$ than with controlling systematic errors. A small value of $\overline{\psi_n}$ implies that anomaly estimation errors are small compared to the variance of the anomalies themselves. For the analyses presented here, we use only a subset of the 175 basins for which $\overline{\psi_n}$ is less than 0.25; this value is chosen as the smallest value that will still leave a reasonable number of basins in the tropics and high latitudes. Additionally, we accept only those basins for which the characteristic relative error in long-term basin mean annual precipitation (ψ_a) is less than 0.5. This value is chosen to remove only the most seriously biased cases, because bias will affect our assessment only indirectly. The constraint on $\overline{\psi_n}$ reduced the data set to 134 basins, and the constraint on ψ_a reduced it further to 124. Of the 124 basins, 19 are within 30° of the Equator, and 18 are poleward of 55°N.

2.2. Air Temperature

[10] Station records of air temperature were obtained from Global Historical Climatology Network (GHCN) version 2, produced jointly by the National Climatic Data Center and the Carbon Dioxide Information Analysis Center. The data are expressed as monthly mean values from about 7000 stations worldwide. GHCN temperature data

have been subjected to an extensive set of quality-control procedures [*Peterson et al.*, 1998]. The station records were used to estimate long-term annual-mean basin mean temperature, following exactly the procedures described in part 1 for precipitation.

2.3. Climate-Model Outputs

[11] We complemented our observational data with outputs of unobservable variables from a global model of the land-atmosphere-ocean system. The model is the medium-resolution (3.75° longitude by 2.25° latitude land grid) climate model used by *Knutson et al.* [1999], and the experiment is their 1000-year control run, which represents a steady state climate approximating that of the present-day. The land component of the model [*Manabe*, 1969] tracks water storage in a snowpack reservoir and a root zone reservoir. The root zone reservoir receives water from rainfall and snowmelt and loses water by evaporation and runoff; runoff occurs when necessary to prevent root zone storage from exceeding the root zone soil water capacity, which is a parameter of the model. For this analysis, we used monthly-mean model outputs of rainfall, snowfall, snowmelt, and runoff. Outputs on the model grid were averaged over basin areas by use of the basin masks described in part 1.

3. Theoretical Framework

3.1. Power Spectral Density and Gain Functions

[12] The temporal variability of any variable $x(t)$ (such as river discharge) can be characterized in the frequency domain by use of the power spectral density function (power spectrum), which is defined as the Fourier transform of the autocorrelation function of $x(t)$,

$$\Phi_{xx}(\omega) = \int_{-\infty}^{\infty} \phi_{xx}(t)\exp(-j\omega t)dt, \tag{3}$$

in which $\phi_{xx}(t)$ is the autocorrelation function,

$$\phi_{xx}(t) = \mathrm{E}[x(t')x(t'-t)], \tag{4}$$

where E[ ] is the expectation operator and t' is any time. The integral of $\Phi_{xx}(\omega)$ over all frequencies ω yields the variance of the process $x(t)$, and the function $\Phi_{xx}(\omega)$ expresses the relative contribution of variability at any frequency ω to the total variance. For time averages x_τ over some period τ, the variance of x_τ is equal to the integral of $\Phi_{xx}(\omega)$ from 0 to the frequency associated with τ,

$$\sigma_\tau^2(x) = \int_0^{2\pi/\tau} \Phi_{xx}(\omega)d\omega. \tag{5}$$

Herein we use the notation $\sigma_m^2(x)$ and $\sigma_a^2(x)$ to denote variances of monthly and annual values of a variable x, respectively.

[13] The power spectrum can also be related to the Fourier transform of $x(t)$,

$$\Phi_{xx}(\omega) = 2\pi|X(\omega)|^2, \tag{6}$$

in which $X(\omega)$ is the Fourier transform of $x(t)$. We consider a linear input-output relation of the form

$$o(t) = \int_{-\infty}^{t} i(\tau)h_{io}(t-\tau)d\tau, \tag{7}$$

in which $i(t)$ is the input, $o(t)$ is the output, and $h_{io}(t)$ is the impulse response function that describes the output that would result from a unit impulse input at time 0. Application of the Fourier transform yields the simple relation

$$O(\omega) = 2\pi H_{io}(\omega)I(\omega), \tag{8}$$

in which upper-case letters denote transforms. The function $2\pi|H_{io}(\omega)|$ controls the amplification or attenuation of a signal of a given frequency in the conversion of an input to an output by the response function $h_{io}(t)$. Combination of (6) and (8) yields

$$\Phi_{oo}(\omega) = G_{io}(\omega)\Phi_{ii}(\omega), \tag{9}$$

in which we have introduced the gain function, $G_{io}(\omega)$, defined by

$$G_{io}(\omega) = 4\pi^2|H_{io}(\omega)|^2. \tag{10}$$

3.2. Decomposition of the Discharge Power Spectrum

[14] In this paper, we view river discharge as the final output of a series of linear processes having the form (7). This may seem to be an extreme point of view, given the often emphasized nonlinearity of hydrologic processes. However, linear theory is being applied here only to anomalies, or departures from the long-term mean seasonal water balance, and is not being used to predict that balance itself. We simply assume that anomalies are sufficiently small to be approximated by linear relations. One factor contributing to the viability of this linearization is the fact that spatial and temporal averaging of local, heterogeneous, nonlinear processes can produce nearly linear processes at larger scales. Ultimately, the internal consistency and physical plausibility of the results obtained here must be considered in evaluating the usefulness of this assumption.

[15] The following variables are assumed to be related linearly by sequential relations of the form (7): precipitation (rainfall plus snowfall) rate $p(t)$, effective rainfall (liquid precipitation plus snowmelt) rate $l(t)$, runoff rate $q(t)$, and basin discharge rate $y(t)$. The first three variables are basin mean values of point fluxes. In basins without snow, $p(t)$ and $l(t)$ are identical; in snow-affected basins, the transformation of $p(t)$ to $l(t)$ describes, in an average way, the temporary storage of snow as snowpack. Runoff here refers to soil water excess, which may manifest itself as downward or lateral drainage of the root zone or as surface runoff associated with saturation of the soil surface. The conversion of runoff to discharge is controlled by basin storage, which includes storage as groundwater (below the root zone) and surface water (streams, swamps, lakes, etc.). For this study, these reservoirs are lumped together, because observational data for their separation are not generally available. We

Table 1. Characteristics of Representative River Basins

River	Gauge Location	Latitude of Basin Centroid, °N	Basin Area, km^2	Basin Annual Precipitation, mm	Basin Annual Mean Temperature, °C
Pechora	Ust' Tsil'ma (Russia)	65	248,000	760	−3
Göta älv	Vänersborg (Sweden)	59	47,000	750	5
Susquehanna	Harrisburg (Pennsylvania, USA)	41	62,000	1,110	9
Danube	Orsova (Romania)	47	576,000	965	9
Nueces	Three Rivers (Texas, USA)	29	40,000	610	21
Magdalena	Puerto Berrío (Colombia)	4	74,000	2,100	19

acknowledge our neglect of the effects of a plant canopy; a canopy may affect the net partitioning of precipitation into runoff and evaporation, but is not expected to store appreciable amounts of water at the monthly timescale. Our model contains no representation of the infiltration-excess mechanism of runoff production.

[16] Application of the linear-response model to this series of variables implies that the power spectrum of discharge is the product of the power spectrum of precipitation and a series of terms describing frequency-dependent filtering of the precipitation signal through the snowpack, root zone, and basin store,

$$\Phi_{yy}(\omega) = \Phi_{pp}(\omega) G_{pl}(\omega) G_{lq}(\omega) G_{qy}(\omega), \tag{11}$$

In order to inject some of our understanding of low-frequency control of discharge into the analysis, it is helpful to recast (11) as

$$\Phi_{yy}(\omega) = \Phi_{pp}(\omega) G_{py}(0) \left(\frac{G_{pl}(\omega)}{G_{pl}(0)}\right) \left(\frac{G_{lq}(\omega)}{G_{lq}(0)}\right) \left(\frac{G_{qy}(\omega)}{G_{qy}(0)}\right), \tag{12}$$

in which

$$G_{py}(0) \equiv G_{pl}(0) G_{lq}(0) G_{qy}(0). \tag{13}$$

Our introduction here of zero-frequency values is a convenient artifice that anticipates our findings that these factors tend to be independent of frequency at sufficiently low frequency. In practice, we can then estimate the zero-frequency term as an average value over frequencies less than some threshold value (e.g., 1 y^{-1}).

[17] Equation (12) provides the theoretical framework for this paper, whose objective is to explore the contribution of the five factors on the right side of the equation to the variability of discharge. We examine each quantity in turn, using observational data to the extent possible, but complementing the data, where necessary, with information derived from numerical modeling. We begin the analysis with a description of the prominent features of $\Phi_{pp}(\omega)$ and $\Phi_{yy}(\omega)$, which describe the frequency dependence of variations in precipitation and discharge anomalies, based solely on observational data. We then show how the results of part 2 yield an accurate, observationally based predictor of $G_{py}(0)$, which characterizes sensitivity of long-term mean discharge to long-term mean precipitation. The factor containing $G_{pl}(\omega)$, which quantifies the role of snow storage and snowmelt in the conversion of precipitation variability to variability of effective rainfall, is estimated from numerical simulations of the snowmelt process in the framework of a climate model. The factor containing $G_{lq}(\omega)$, which characterizes the role of soil water in converting effective rainfall variability to that of runoff, is also viewed from a modeling perspective. Finally, the term involving $G_{qy}(\omega)$, which represents the effect of basin storage on conversion of runoff variability to discharge variability, is evaluated as a residual, given estimates of the other quantities in (12). The result is used to parameterize a simple linear basin storage model, and some physical controls on the model residence time are identified.

[18] The combined use of observational and model-generated data is less realistic than exclusive use of observational data. This is an unavoidable feature of the analytic approach that we have chosen. Any systematic errors that may be present in the gain functions derived from the model would translate to corresponding errors in the inferred gain function describing basin storage. As we shall see, however, the factors evaluated by use of the model generally appear to contribute relatively little to discharge variability. Furthermore, only the shapes of these functions are derived from the model; their absolute levels are set on the basis of observational and theoretical considerations.

4. Analysis

4.1. Representative Basins

[19] Given the large number of basins in the study, we cannot display the various power spectral density functions for all basins. For this reason, we instead devote many figures to the display of various integral measures of the spectral characteristics. Such summary measures, however, hide much of the interesting detail. Accordingly, we have chosen to display also various power spectra for a selection of six representative basins. The basins were chosen to represent ''end-members'' of behaviors that were noted across the full population of basins. Characteristics of the selected representative basins are presented in Table 1. The basins of the Pechora and Göta älv Rivers are in the high latitudes of northern Europe; the latter basin contains a large lake that strongly conditions the discharge characteristics. The Danube and Susquehanna River Basins are representative of middle-latitude basins. The Nueces and Magdalena River Basins are representative of hot/dry and hot/moist basins, respectively, of the low latitudes.

4.2. Spectra of Observed Precipitation and Observed Discharge

[20] Representative power spectra of observed precipitation and discharge are presented in Figure 1. Most precipitation spectra contain approximately equal power at all frequencies, with no apparent spectral peaks associated with such physical phenomena as ENSO. The most frequently

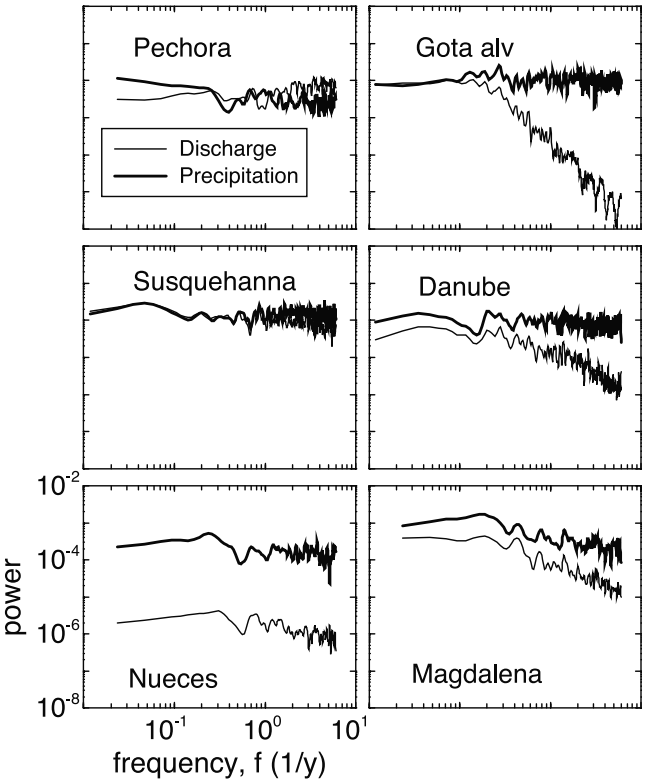

Figure 1. Power spectra of observed precipitation and discharge for representative basins.

observed departure from uniform spectra (“white noise”) is exemplified by the Magdalena River Basin, for which the precipitation spectrum shows a gradual decrease in power with increasing frequency (“red noise”). Discharge spectra exhibit either relatively small departures from white noise (Pechora, Susquehanna, Nueces) or distinctly red noise character (Göta älv, Danube, Magdalena).

[21] A quantitative measure of the shape of the precipitation power spectrum is a normalized ratio of the variance of monthly mean precipitation rate anomalies to annual mean rate anomalies, $\sigma_m^2(p)/12\sigma_a^2(p)$. For a white noise process, with equal power at all frequencies, this ratio would have a value of unity, as can be shown by means of (5). A value of this ratio smaller than unity is indicative of red noise and implies persistence (positive autocorrelation) in monthly precipitation anomalies. Figure 2 shows a slight reduction in power (relative to white noise) at the higher frequencies for most of the precipitation spectra; the value of the index for the many mid-latitude basins is between 0.6 and 1. Near-equatorial precipitation spectra, with most index values about 0.4 to 0.6, are much redder than midlatitude spectra; this redness implies a greater tendency for persistence of monthly anomalies of basin mean precipitation in near-equatorial basins. The data also suggest a slight increase in redness of precipitation spectra (increase in autocorrelation of monthly precipitation) at high latitudes. In three high-latitude basins, however, the index for discharge is substantially greater than 1, which implies the presence of “blue noise” (relatively high power at high frequencies). No systematic dependence of spectrum shape on the basin area was found; the redness of precipitation spectra did not appear to be scale-dependent.

[22] The basins in Figure 1 highlight some of the main characteristics of the relation between precipitation and discharge spectra. In simplest terms, for most basins, transformation of precipitation variability to discharge variability can be viewed as the combination of two steps. The first of these is a constant reduction in variability at all frequencies, apparent as a vertical displacement of the discharge spectrum relative to the precipitation spectrum. The second is a frequency-dependent decrease in variability (reddening of the spectrum) that is absent at low frequency and increasingly apparent at high frequencies; this decrease in variability can be seen as a “bending” of the vertically displaced precipitation spectrum that would be necessary to obtain the discharge spectrum. In the Pechora and Susquehanna River Basins, both of these transformations are relatively small; indeed, high-frequency variability of discharge even exceeds that of precipitation in the former basin (and in several other high-latitude basins). In the Göta älv River Basin, no attenuation occurs at low frequency, but strong reddening occurs at high frequencies. In the Magdalena and Nueces River Basins, the all-frequency reduction in variability is more apparent than the reddening. Both types of attenuation are apparent for the Danube River Basin.

[23] Values of $\sigma_m^2(p)/12\sigma_a^2(y)$ plotted in Figure 2 are typically in the range 0.2–0.4 and are, therefore, much lower than the corresponding values for precipitation. The substantial and systematic downward vertical displacement of the discharge data points from the precipitation data points in Figure 2 is a measure of the reddening of discharge spectra relative to precipitation spectra. It is apparent that a relative reddening of discharge spectra is almost universal from the Equator through the middle latitudes. In the high latitudes, the redness of discharge spectra varies over a much wider range than the redness of precipitation spectra. For some high-latitude basins (for example, the Pechora River Basin), the discharge spectrum is less red than the precipitation spectrum, which reflects a relative increase in high-frequency variability of discharge over that of precipitation for those basins.

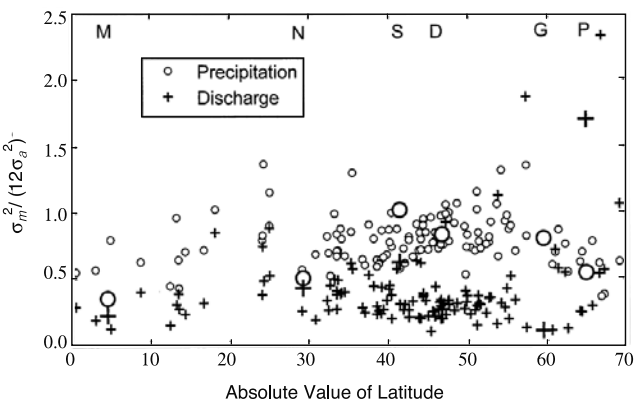

Figure 2. Scatterplot of $\sigma_m^2(p)/12\sigma_a^2(p)$ and $\sigma_m^2(y)/12\sigma_a^2(y)$ as a function of absolute value of mean basin latitude. Departure below unity is a measure of the redness of the respective process. Enlarged symbols represent the six sample basins, identified by a letter at the top of the figure, above the corresponding symbol: M, Magdalena; N, Nueces; S, Susquehanna; D, Danube; G, Göta älv; P, Pechora.

[24] To facilitate an overview of the relative reddening of the discharge spectrum by surface processes, we show in Figure 3 the ratio of the discharge and precipitation redness indices that were plotted in Figure 2. This is a measure of the extent to which high-frequency fluctuations are damped more than low-frequency fluctuations in the transformation from precipitation to discharge. From the Equator through the middle latitudes, discharge spectra in this data set are uniformly redder than precipitation spectra. The ratio of discharge redness to precipitation redness varies more at high latitudes than elsewhere. Values of this ratio are even greater than 1 for several basins, indicating that the discharge spectrum is less red than the precipitation spectrum; the Pechora River Basin has already been noted as an example of such behavior. Figure 3 suggests that this phenomenon may be correlated with the occurrence of an annual mean air temperature that is lower than the freezing point of water. We shall return to this observation later.

4.3. Low-Frequency Response

[25] A consistent feature of nearly all basins is near-parallelism (pure vertical offset without bending) of precipitation and discharge spectra at low frequencies (i.e., typically for timescales of 1 year and longer). This feature implies frequency-independent transformation (preservation or reduction) of precipitation variability to discharge variability at low frequencies. Within this low-frequency regime, the difference between precipitation and discharge variability (the vertical shift mentioned earlier) is highly variable across basins. In some basins (e.g., Susquehanna), discharge variability is nearly equal to precipitation variability. In others (e.g., Nueces), discharge variability is one or more orders of magnitude smaller than that of precipitation. A measure of the difference in low-frequency variability between discharge and precipitation is the ratio

$$\frac{\int_0^{\omega_a} \Phi_{yy}(\omega)d\omega}{\int_0^{\omega_a} \Phi_{pp}(\omega)d\omega} = \frac{\sigma_a^2(y)}{\sigma_a^2(p)}, \tag{14}$$

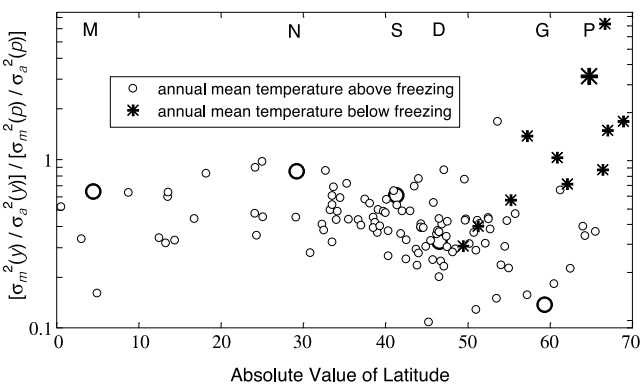

Figure 3. Scatterplot of the ratio $[\sigma_m^2(y)/\sigma_a^2(y)]/[\sigma_m^2(p)/\sigma_a^2(p)]$, which indicates the reltive damping of high frequencies in the transformation of precipitation to discharge. Enlarged symbols represent the six sample basins, identified by a letter at the top of the figure, above the corresponding symbol: M, Magdalena; N, Nueces; S, Susquehanna; D, Danube; G, Göta älv; P, Pechora.

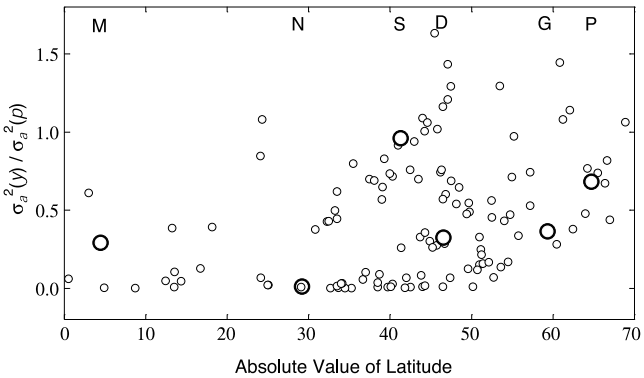

Figure 4. Scatterplot of the ratio $\sigma_a^2(y)/\sigma_a^2(p)$ as a function of absolute value of mean basin latitude. This ratio quantifies the attenuation of discharge variability relative to that of precipittion at low frequencies. Enlarged symbols represent the six sample basins, identified by a letter at the top of the figure, above the corresponding symbol: M, Magdalena; N, Nueces; S, Susquehanna; D, Danube; G, Göta älv; P, Pechora.

in which ω_a is 2π/(1 year). A scatterplot of this quantity against latitude is presented as Figure 4, which shows a very wide range of values from near zero in some low- and middle-latitude basins to near one and even greater in some middle- and high-latitude basins. Also notable, however, is the large variance of the index at most latitudes. In the middle latitudes, the distribution of the index is bimodal, with a cluster of values near 0 (generally arid basins) and a spread of values above 0.5 (humid basins).

[26] In part 2 it was shown that, to a good approximation, observed low-frequency (annual and longer timescale) variations of discharge are mainly a response to low-frequency precipitation variations, with the sensitivity dependent on *Budyko*'s [1974] index of dryness, as originally suggested in the context of numerical model experiments [*Koster and Suarez*, 1999]. Accordingly,

$$\frac{\sigma_a^2(y)}{\sigma_a^2(p)} = \left(\frac{dY_n}{dP_n}\right)^2, \tag{15}$$

where $\frac{dY_n}{dP_n}$ denotes the sensitivity of total discharge in water year $n(Y_n)$ to total precipitation in the same year (P_n). To evaluate this sensitivity, we introduce the semiempirical relation

$$\overline{Y}/\overline{P} = 1 - \phi(\zeta), \tag{16}$$

in which ζ is the climatic index of dryness (ratio of long-term mean radiation, expressed as equivalent evaporative flux, to long-term mean precipitation). Multiple functional forms have been proposed for $\phi(\zeta)$. Although we found in part 2 that the form of *Budyko* [1974] may be somewhat biased, we chose to use it here; results obtained herein are insensitive to the choice of $\phi(\zeta)$. Thus, we have [*Budyko*, 1974]

$$\left(\overline{Y}/\overline{P}\right)_B = 1 - \left[\zeta\left(\tanh\zeta^{-1}\right)(1 - \cosh\zeta + \sinh\zeta)\right]^{1/2}, \tag{17}$$

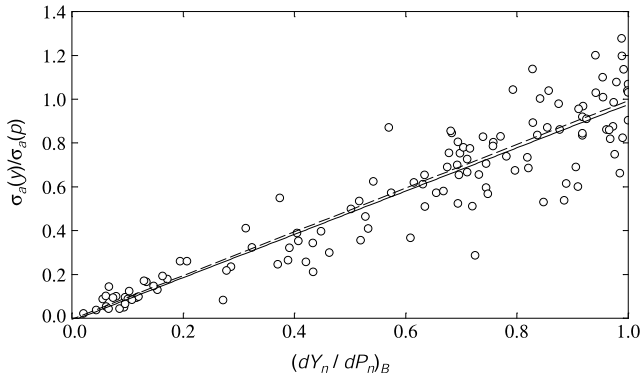

Figure 5. Scatterplot of the ratio of annual standard deviations $\sigma_a(y)/\sigma_a(p)$ against $(\frac{dY_n}{dP_n})_B$ given by (19) and (17). Solid line is least squares fit ($y = -0.012 + 0.998x$; $r = 0.92$), and dashed line is 1:1 line.

where the subscript B indicates use of Budyko's $\phi(\zeta)$. With the approximation that

$$\frac{dY_n}{dP_n} = \frac{d\overline{Y}}{d\overline{P}}, \tag{18}$$

we have also

$$\left(\frac{dY_n}{dP_n}\right)_B = 1 - \frac{1}{2}\left[\zeta^{-1}\tanh\zeta^{-1}\left(1-e^{-\zeta}\right)\right]^{-1/2}\left[\tanh\left(\zeta^{-1}\right)\right.$$
$$\left.\left(1-e^{-\zeta}-\zeta e^{-\zeta}\right)+\zeta^{-1}\left(\operatorname{sech}\zeta^{-1}\right)^2\left(1-e^{-\zeta}\right)\right]. \tag{19}$$

Together, (19) and (17) yield $\left(\frac{dY_n}{dP_n}\right)_B$ as a function of the observed $\overline{Y}$ and $\overline{P}$. The ability of (15), (19), and (17) to predict the ratio in annual variances for the present data set is shown in Figure 5.

[27] Under the approximation, supported by Figure 1 and equivalent plots for the other basins, that precipitation and discharge spectra are parallel for frequencies below ω_a, it follows from (15) that

$$\Phi_{yy}(\omega) = \left(\frac{dY_n}{dP_n}\right)_B^2 \Phi_{pp}(\omega), \quad \omega \le \omega_a. \tag{20}$$

This relation implies that

$$G_{py}(0) = \left(\frac{dY_n}{dP_n}\right)_B^2. \tag{21}$$

[28] We have identified a convenient model for $G_{py}(0)$, but the relative contributions of snowpack, root zone, and basin storage have not been identified. Such a decomposition, of course, is not possible when only precipitation and discharge data are used, but requires also accurate observations of basin mean snowpack, root zone soil water, and groundwater and surface water storage. Lacking such data, we can nevertheless make some judgments about the roles of the various reservoirs. At very long timescales (i.e., in the limit as ω goes to 0), we expect storage rates in snowpack, soil, surface water, or groundwater to be insufficient to affect variances of the respective outflows from these reservoirs, so that outflows will be effectively in phase with inflows. (This expectation does not apply to glaciers, whose long response times necessarily exclude them from our analysis.) If the rate of water flowing out of the snowpack and groundwater and (natural or man-made) surface water reservoirs were essentially equal to the respective inflow rates (or, more precisely, if losses from these reservoirs were independent of inflow), it would follow that $G_{pl}(\omega)$ and $G_{qy}(\omega)$ go to 1 for sufficiently small ω. In contrast, we suppose that low-frequency changes in inflow to the root zone will result in changes both in outflow (runoff) and in root zone evaporation. Such assumptions are perhaps valid in most environments, but inadequate in particular cases. As an approximation, then, we expect that

$$G_{py}(0) = G_{lq}(0), \tag{22}$$

$$G_{pl}(0) = G_{qy}(0) = 1, \tag{23}$$

i.e., that the net low-frequency effect of all reservoirs in the basin can be attributed to the soil water reservoir.

4.4. Snowpack Storage

[29] To estimate the contribution to discharge variability that is associated with snow storage, the model-derived time series of precipitation and effective rainfall were analyzed. Sample spectra are plotted in Figure 6. The spectra show that the effect of snow is absent or negligible in the Magdalena, Nueces, Danube, and Susquehanna River Basins. These are basins in which the change of snowpack mass is a small term

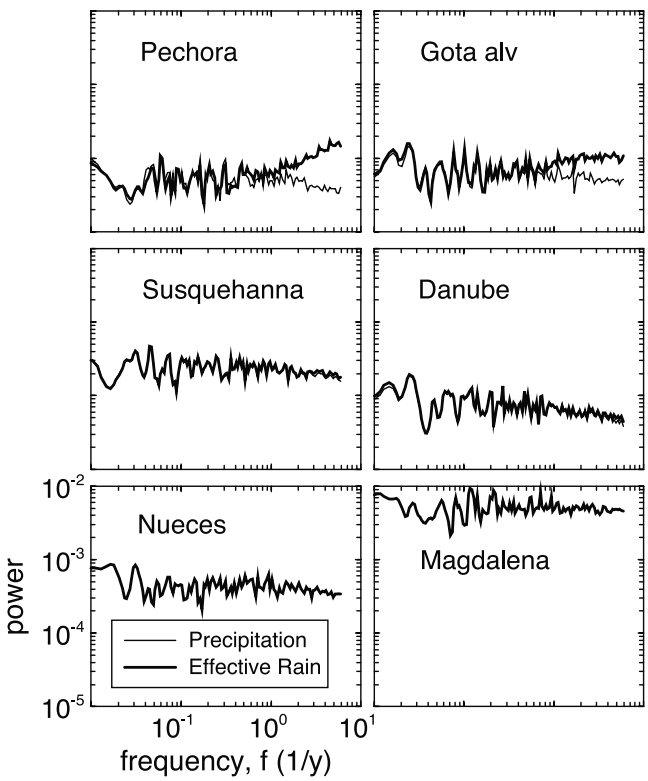

Figure 6. Power spectra of model output precipitation and effective rainfall for representative basins.

in the monthly water balances of the model basins. In contrast, the effect of snow storage is apparent in the two most northern of the sample basins, the Pechora and the Göta älv River Basins. Even in these basins, at frequencies corresponding to periods greater than 1 year, the precipitation and effective-rainfall spectra are nearly identical. This result supports our earlier assumption that dynamic, interannual storage of snow is negligible in non-glaciated basins. At higher frequencies, however, an increasing amplification of variability of effective rainfall, relative to that of precipitation, is apparent. This increase can be attributed to the combination of two factors: (1) the short-term release, by melting, of precipitation accumulated during the entire snowfall season, and (2) the variability in timing of this short snowmelt period, which is associated with the variability in energy availability from year to year. The heightened variability of discharge at the shortest (monthly) timescale implies a negative lag-1 autocorrelation in the process at that timescale. Thus, for example, if snowmelt in April is greater than normal, then snowpack and potential for snowmelt will be less than normal in May. Our results are consistent with those of *Delworth and Manabe* [1988], which were based on spectral analysis of precipitation output from a similar model. They showed that the fraction of variability associated with high frequencies was greater for effective rainfall than for precipitation at high latitudes.

[30] Figure 7 is a plot against latitude of the ratio $\sigma_m^2(I)/\sigma_m^2(p)$, which expresses the contribution to discharge variability associated with snow storage and melting. Figure 7 shows that the influence of snow on the spectra of effective precipitation has a clear zonal dependence. It also shows, for a given latitude, that the magnitude of the effect increases with the fraction of annual precipitation falling as snow. This amplification of high-frequency variability in high latitudes, inferred from model output, is one factor helping to explain the latitudinal variation in reddening of discharge spectra relative to precipitation spectra (Figure 3).

4.5. Soil Water Storage

[31] We first investigate the effect of soil water storage on discharge variability by computing, for the model, the ratio

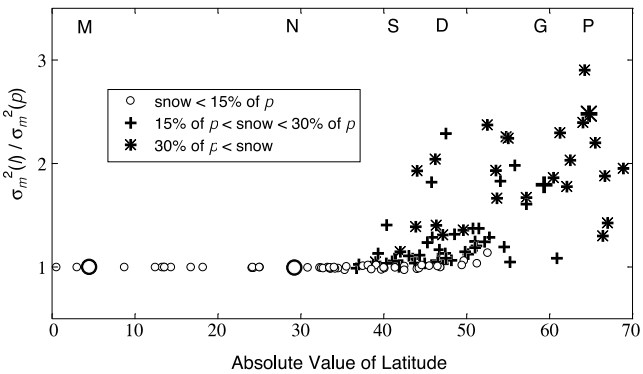

Figure 7. Scatterplot of the ratio $\sigma_m^2(I)/\sigma_m^2(p)$ against absolute value of mean basin latitude. This ratio quantifies the amplification of effective rainfall variability relative to that of precipitation. Enlarged symbols represent the six sample basins, identified by a letter at the top of the figure, above the corresponding symbol: M, Magdalena; N, Nueces; S, Susquehanna; D, Danube; G, Göta älv; P, Pechora.

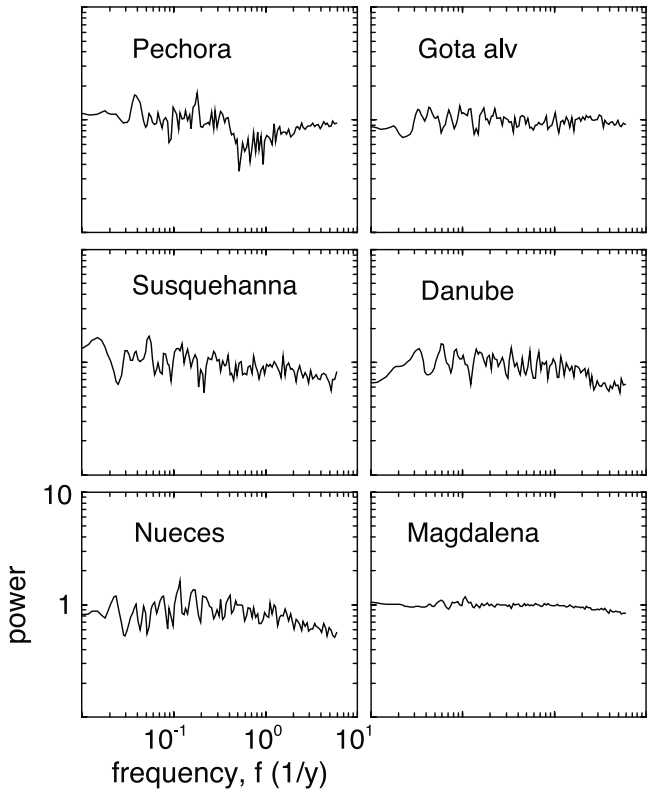

Figure 8. Model-derived estimates of $G_{lq}(\omega)/G_{lq}(0)$ for representative basins. This ratio reflects the frequency dependence of the transformation of infiltration variability to runoff variability. ($G_{lq}(0)$ was estimated as the average value of $G_{lq}(\omega)$ over frequencies less than ω_a.)

$G_{lq}(\omega)/G_{lq}(0)$ (Figure 8). This quantity reflects the contribution of root zone water balance dynamics to the relative reddening of the discharge power spectrum. In the middle- and low-latitude basins, a relatively small increase in redness can be detected. A simple measure of this tendency is the ratio of $\sigma_m^2(q)/\sigma_a^2(q)$ to $\sigma_m^2(I)/\sigma_a^2(I)$. Perfectly parallel spectra of effective rainfall and runoff would produce a value of unity for this ratio. Relative reddening of runoff by soil water storage would produce values smaller than unity. The distribution of this measure with latitude is shown in Figure 9. In the low and high latitudes, values of this index scatter around 1, implying no systematic reddening of the signal by soil moisture. In the middle latitudes, values average about 0.8, implying a moderate damping of the higher frequencies.

[32] In addition to their analysis of model precipitation spectra, mentioned above, *Delworth and Manabe* [1988] also examined soil moisture spectra. They noted that nearly white precipitation input led to a red soil moisture spectrum, with strong damping of soil moisture fluctuations at the monthly timescale. Given the strong connection between soil moisture and runoff in the model, the relative absence of redness in the runoff spectrum noted here may at first seem surprising. In fact, soil moisture persistence in the model is associated with seasons when the soil is usually not saturated, as a result of an excess of evaporative demand over precipitation. In the model, runoff occurs only in seasons when the soil reservoir is saturated, at which time soil moisture has very short timescales. Thus, the runoff

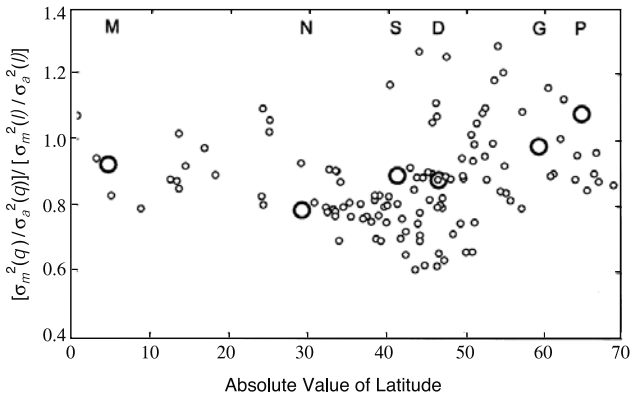

Figure 9. Scatterplot of model output ratio of $\sigma_m^2(q)/\sigma_a^2(q)$ to $\sigma_m^2(l)/\sigma_a^2(l)$ against absolute value of mean basin latitude. The proximity of values to unity indicates that soil water storage contributes little to the reddening of the runoff spectrum. Enlarged symbols represent the six sample basins, identified by a letter at the top of the figure, above the corresponding symbol: M, Magdalena; N, Nueces; S, Susquehanna; D, Danube; G, Göta älv; P, Pechora.

parameterization is highly selective in sampling soil moisture variability. The net result is that soil moisture, at least in this model parameterization, contributes very little to modification of the shape of the power spectrum in the transition from effective precipitation to runoff.

4.6. Effect of Groundwater and Surface Water Storage on Discharge Variability

[33] We now use (12) to obtain an estimate of the combined effect of groundwater and surface- water storage on the variability of discharge. We solve (12) for $\frac{G_{qy}(\omega)}{G_{qy}(0)}$, using observations to evaluate the precipitation and discharge spectra $\Phi_{pp}(\omega)$ and $\Phi_{yy}(\omega)$, and the model-derived estimates of $\frac{G_{pl}(\omega)}{G_{pl}(0)}$ and $\frac{G_{lq}(\omega)}{G_{lq}(0)}$. To evaluate $G_{py}(0)$, we use (21), with (19), (17), and the observations of long-term means of y and p. Note that the most important terms in (12) are thus evaluated from the observations, and that the two model-evaluated factors are only weakly dependent on frequency. We expect this to lead to a fairly accurate estimate of $\frac{G_{qy}(\omega)}{G_{qy}(0)}$.

[34] Results are shown in Figure 10. The degree of relative attenuation of high-frequency variability by groundwater and surface water varies widely from one basin to another. In most basins, discharge variability is less than runoff variability at monthly to annual timescales. In many high-latitude basins (e.g., Pechora), and in many arid basins (e.g., Nueces) almost no filtering occurs. In other basins (e.g., Göta älv), even interannual runoff variations are notably damped in the production of discharge.

[35] The degree of attenuation of runoff variations by the basin is readily characterized in terms of a basin residence time of water associated with a simple model of combined groundwater and surface water storage. Let outflow from this combined store (which is discharge, y) be proportional to storage, S

$$y = -S/\tau \tag{24}$$

and let inflow to the store be given by the runoff rate q. For this simple development, we shall ignore the loss of water from groundwater and surface water by evaporation, in accordance with an earlier assumption. Then

$$\frac{dS}{dt} = q - S/\tau. \tag{25}$$

By taking a time average of (25) at equilibrium, we can see that τ is the ratio of average throughflow rate to average storage; it can thus be viewed as an average residence time of water.

[36] For this simple storage model, it can be shown, using the methods of section 3.1. that

$$G_{qy}(\omega) = \frac{1}{1 + (\omega\tau)^2}. \tag{26}$$

We have fitted this expression to the data for each basin, forcing preservation of the ratio of monthly to annual integrals of the spectrum. Results for the sample basins are shown in Figure 10. For some basins, (26) cannot satisfy this constraint, and was simply set to zero, allowing full passage of high-frequency variability. The non-zero fitted residence times range from near 0 to more than1 year; most values are in the 10- to 60-day range. In the next section we examine controls on this effective basin residence time.

4.7. Controls on Effective Basin Residence Time

[37] Figure 11 shows the fitted values of τ plotted against latitude. In the tropics, values are mostly in the 10- to 100-day range. Values are typically smaller than this, all less

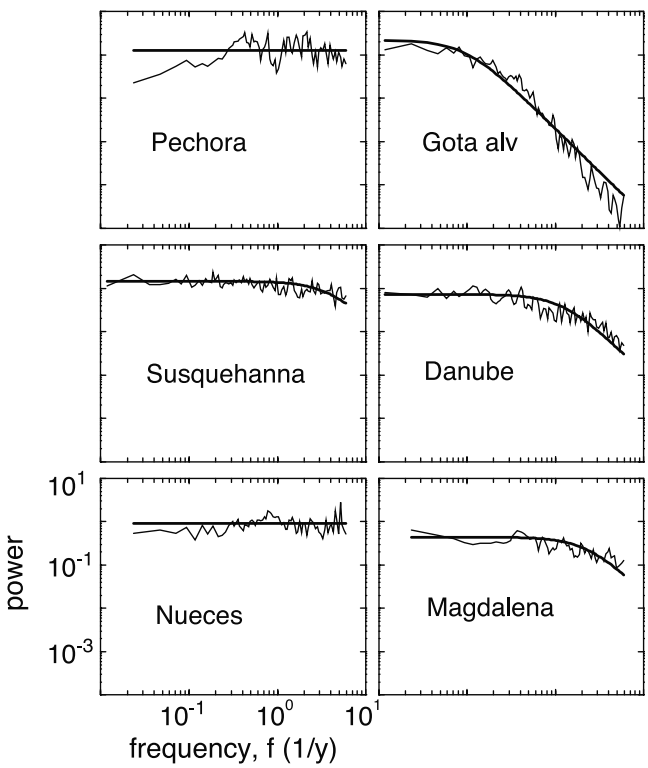

Figure 10. Estimated $\frac{G_{qy}(\omega)}{G_{qy}(0)}$ for representative basins, reflecting frequency-dependent attenuation of discharge variability by groundwater and surface water storage. The heavy, smooth curve is the best fit of the form (26).

than 30 days, in the subtropics. North of the subtropics, the median value tends to increase with latitude through the middle latitudes. In the high latitudes, the variance of τ is very large, with both the largest and smallest values found in this zone.

[38] The presence of substantial lake area in a basin appears to explain many of the large values of τ (Figure 11). Lakes greatly increase the surface area of surface water in a basin, permitting relatively large changes in storage volume for a given rise in discharge. By (24), this fact implies that the presence of lakes tends to increase the value of τ. Figure 11 shows that seven of the nine largest values of τ are associated with basins in which lakes are estimated to cover more than 5% of the basin area; overall, only 16 of the 124 basins studied had such large fractional lake areas. The strong damping of variability in the Göta älv River Basin, one of our representative basins, can be understood in terms of lake storage (Vänern Lake). Other lake-affected basins in our data set include the St. Lawrence (Great Lakes, τ = 360 d), the Neva (Lake Ladoga, τ = 320 d), the Nelson (Lake Winnipeg, τ = 150 d), and the White Nile (Lake Victoria, τ = 160 d) River Basins.

[39] We investigated further the two basins with τ greater than 100 days that did not have estimated fractional lake areas greater than 5%. The investigation revealed that these basins were "exceptions that prove the rule." In both basins our estimates of fractional lake area were far too low as a result of our use of a 1° basin map to represent small basins. In fact, these basins should have been grouped with the other lake-affected basins.

[40] We found another strong control on high-latitude variance of τ to be the presence of freezing conditions. Figure 11 shows that the low values of τ in high latitudes are associated with occurrence of annual mean temperatures below the freezing point of water. Very approximately, regions of sub-freezing mean temperature tend to be regions of continuous or discontinuous permafrost [*Lunardini*, 1981]. Among our sample basins, the Pechora River Basin (annual mean temperature of −3 C, τ = 1 d) is representative of the freezing-affected basins. Other such basins include the Koyukuk River Basin in Alaska (−6 C, τ = 0), and the Lena (−8 C, τ = 0) and Yenisey (−4 C, τ = 5 d) River Basins in Siberia.

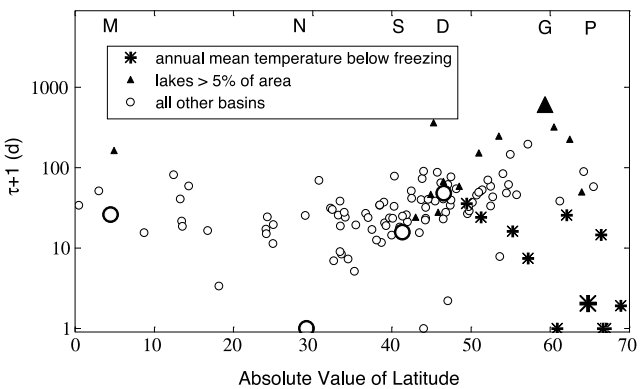

Figure 11. Scatterplot of effective basin residence time against absolute value of mean basin latitude. (We plot τ + (1 d) in order to permit use of a log scale.) Enlarged symbols represent the six sample basins, identified by a letter at the top of the figure, above the corresponding symbol: M, Magdalena; N, Nueces; S, Susquehanna; D, Danube; G, Göta älv; P, Pechora.

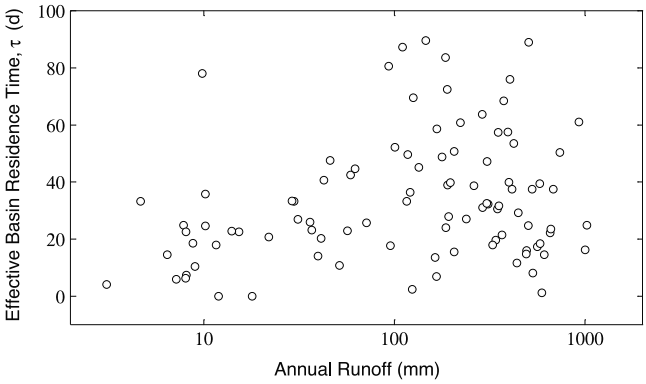

Figure 12. Scatterplot of effective basin residence time τ against runoff rate. Basins with more than 5% area covered by lakes and/or with annual-mean temperature below freezing are excluded. (For two basins, not plotted, τ is between 100 and 200 d and annual runoff is between 200 and 300 mm.)

[41] We hypothesize that the widespread presence within a basin of a frozen soil layer presents a barrier to exchange between surface and near-surface water (including the unfrozen "active layer" of the soil) and the deeper subsurface. The loss of this major storage reservoir makes discharge of cold-region basins respond much more rapidly than that of other basins. Our conclusions are consistent with field analyses of *Haugen et al.* [1982], who compared the hydrologic responses of research watersheds in Alaska. They concluded that areas underlain mainly by permafrost have a "flashier" response to precipitation than mostly non-permafrost areas in the same basin. It is likely that the spring breakup of river ice is another factor explaining the connection between freezing conditions and extremely low values of τ.

[42] Having found that extreme values of τ may be explained by presence of lakes or freezing conditions, we subsequently excluded such extreme basins from the data set and examined the influence of other physical factors. We found no strong controls by measures of topography (variance of elevation in the basin) or soil texture (fractional coverage by fine, medium, or coarse soils); however, a statistically significant correlation with runoff rate (and runoff ratio, the fraction of precipitation that runs off) was noted (Figure 12). In dry basins, the value of τ is low (0–30 d), as is its variance, but in wetter basins the values are generally higher and have a wider range (0–100 d).

[43] Runoff in arid regions generally does not pass through a saturated groundwater reservoir, because the water table is far below the land surface. Rather, most runoff is produced by high intensity storms and/or on surfaces of low permeability. (That such processes are absent from our model serves as a reminder of the limitations of our analysis.) Thus, arid regions have a flashy response similar to that of permafrost-affected regions, albeit for very different reasons. In humid regions, surface and subsurface waters tend to be in closer hydraulic con-

nection, allowing the considerable storage capacity of the subsurface to dampen fluctuations in runoff.

5. Summary and Discussion

5.1. Summary

[44] We have analyzed, from a global perspective, the climatic and land-process controls on variability of river discharge at monthly and longer timescales. Our approach requires representing anomalies of river discharge as the final result of a series of linear processes, and we focus on the gross features of the frequency dependence of variability. We treat precipitation as the ultimate ''input'' that drives variability of land water fluxes, and we do not address feedbacks from land to atmosphere that may help to define the frequency spectrum of precipitation itself. The power spectrum of water flux variability is continuously reshaped as precipitation is transformed to effective rainfall through snow storage and snowmelt; as effective rainfall is transformed to runoff through the soil water balance; and as runoff is transformed to river discharge through storage and release by groundwater and/or surface water. Given the initial power spectrum of precipitation and the characteristics of each transformation, we can quantitatively assess the influence of each of these processes on discharge variability. Because observational data are not available to quantify some of these processes, we rely on a combination of observational and model-derived estimates of water fluxes.

[45] Our results suggest that most of the character of monthly discharge variability (expressed as a deviation from normal conditions) can be explained in terms of a very simple model. Water flux to land from the atmosphere can be approximated by white noise, with no correlation from one month to the next. Random deviations in water supply produce proportionate deviations in runoff. The constant of proportionality is a function of the long-term runoff ratio of the basin, approaching 0 in arid basins and 1 in very wet basins. Thus, runoff production can also be approximated as white noise, but usually with reduced variance. Finally, storage in the saturated zone and in surface waters acts as a low-pass filter that damps higher frequency discharge variability, but leaves low-frequency variability unmodified from that of runoff production. The strength of the filter, quantified by an effective water residence time, varies widely from one basin to another. Nevertheless, its dependences on freezing conditions in the basin, presence of large lake areas, and overall aridity of the basin are physically realistic.

[46] A minor refinement of this model explains the role played by snow storage. Where a substantial fraction of precipitation falls as snow, the frequency spectrum of effective rainfall departs from the white noise precipitation spectrum. Snow accumulated over many months melts relatively rapidly, and the timing of melt varies from year to year. As a result, the nearly white precipitation spectrum is transformed to a blue noise spectrum of effective rainfall. This transformation, together with the tendency for freezing-induced decoupling of the surface and subsurface, explains the relatively large amount of high-frequency discharge variability observed at high latitudes.

5.2. Distortion of Analysis by Model Outputs

[47] This analysis has been based partly on model outputs rather than observations. Model outputs were the basis for inferences regarding the role of snow storage and snowmelt in the shaping of the discharge spectrum. Given the strong climatic control of these processes, however, it is doubtful that use of a model has introduced any serious error in our evaluation of them.

[48] The model is also the basis for our neglect of the frequency-dependence of the damping of variability by the root zone water reservoir. It is possible that the simplicity of our description of root zone water dynamics hides a larger ''coloring'' of the spectrum by the root zone that might occur in nature. We suspect, however, that the ability of the root zone to shape the spectrum is ultimately limited by its water capacity, which is included in our parameterization. To the extent that we err in ignoring the influence of the root zone, the missing effect would be aliased into our estimates of effective basin residence time.

5.3. Directions for Model Development

[49] Our analysis has some implications for the development of global land models intended to reproduce variability of river discharge at the monthly timescale. Several of our findings point to surface-subsurface interactions as a major land control on discharge variability. It appears that accurate representation of flow variability in cold regions (and perhaps during cold seasons in seasonally freezing regions) requires a description of the restrictions on infiltration caused by frozen subsurface barriers. In arid regions, where most runoff appears to bypass the saturated zone, models must be capable of yielding such surface- or near-surface-generated runoff. In the remaining (not cold, not arid) regions, surface-subsurface interaction can generally be expected, and models must include relevant pathways for flow. In regions with lake or swamp storage, inclusion of such storage in a model is crucial in order to reproduce the extreme damping of high-frequency fluctuations in runoff.

5.4. Disturbed Basins

[50] The focus of this paper has been on natural processes. Basin response may be modified from natural conditions either by changes in land characteristics (e.g., deforestation), or by changes in the ''plumbing'' of the surface water drainage system (e.g., dams). Changes in land characteristics would affect rates of processes treated here, but such changes could generally still be treated within the framework of this analysis. Large changes in the surface-drainage system affect the effective basin residence time. We have found (not shown here) that creation of artificial reservoirs can substantially increase the effective residence time. Similarly, channelization or urbanization may lead to reductions in residence time.

[51] **Acknowledgments.** Krista Dunne provided advice and technical assistance throughout the course of this study. Keith W. Dixon, Peter J. Phillipps, and two anonymous reviewers gave very helpful reviews.

References

Bras, R. L., and I. Rodríguez-Iturbe, *Random Functions and Hydrology*, Addison-Wesley-Longman, Reading, Mass., 1985.

Budyko, M. I., *Climate and Life*, Academic, San Diego, Calif., 1974.

Delworth, T. L., and S. Manabe, The influence of potential evaporation on the variabilities of simulated soil wetness and climate, *J. Clim.*, *1*, 523–547, 1988.

Haugen, R. K., C. W. Slaughter, K. E. Howe, and S. L. Dingman, Hydrology and climatology of the Caribou-Poker Creeks Research Watershed,

Alaska, *Rep. 82-26*, U.S. Army Corps of Engineers, Cold Regions Res. and Eng. Lab., Hanover, N. H., 1982.

Knutson, T. R., T. L. Delworth, K. W. Dixon, and R. J. Stouffer, Model assessment of regional surface temperature trends (1949–1997), *J. Geophys. Res.*, *104*, 30,981–30,996, 1999.

Koster, R. D., and M. J. Suarez, A simple framework for examining the interannual variability of land surface moisture fluxes, *J. Clim.*, *12*, 1911–1917, 1999.

Lunardini, V. J., *Heat Transfer in Cold Climates*, Van Nostrand Rheinhold, New York, 1981.

Manabe, S., Climate and the ocean circulation, 1, The atmospheric circulation and the hydrology of the Earth's surface, *Mon. Weather Rev.*, *97*, 739–774, 1969.

Milly, P. C. D., and K. A. Dunne, Macroscale water fluxes, 1, Quantifying errors in the estimation of basin mean precipitation, *Water Resour. Res.*, *38*(10), 1205, doi:10.1029/2001WR000759, 2002a.

Milly, P. C. D., and K. A. Dunne, Macroscale water fluxes, 2, Water and energy supply control of their interannual variability, *Water Resour. Res.*, *38*(10), 1206, doi:10.1029/2001WR000760, 2002b.

Peterson, T. C., R. Vose, R. Schmoyer, and V. Razuvaev, Global Historical Climatology Network (GHCN) quality control of monthly temperature data, *Int. J. Climatol.*, *18*, 1169–1179, 1998.

P. C. D. Milly and R. T. Wetherald, Geophysical Fluid Dynamics Laboratory, NOAA, Princeton, NJ 08542, USA. (cmilly@usgs.gov)